

A Spectral Low-Mode Reduced Method for Elliptic Problems

Prosper Torsu

Department of Mathematics, California State University Bakersfield
 ptorsu@csusb.edu

ABSTRACT. We develop a spectral low-mode reduced solver for second-order elliptic boundary value problems with spatially varying diffusion coefficients. The approach projects standard finite difference or finite element discretizations onto a global coarse space spanned by the lowest Dirichlet Laplacian eigenmodes, yielding an analytic reduced model that requires no training data and preserves coefficient heterogeneity through an exact Galerkin projection. The reduced solution is energy-optimal in the selected subspace and, for H^2 -regular solutions, the truncation error associated with discarded modes satisfies a $\sqrt{\log M}/M$ decay in the H_0^1 norm. For uniformly stable reduced bases, the projected operator is well conditioned with respect to mesh refinement, and numerical experiments corroborate the predicted accuracy and demonstrate meaningful speedups over sparse direct solvers, with favorable performance relative to multigrid and deflation-based Krylov methods for heterogeneous coefficients in the tested setups.

1. Introduction

The efficient numerical solution of second-order elliptic boundary value problems with spatially varying diffusion coefficients is a fundamental topic in scientific computing [11, 8, 21]. Standard finite difference and finite element discretizations generate large, sparse, symmetric positive definite linear systems [24, 10] whose structure mirrors the underlying coefficient heterogeneity. When meshes are refined or the diffusion coefficient exhibits strong spatial variation, the linear solve often becomes the dominant computational cost [23, 2].

Sparse direct solvers offer robust black-box performance [12, 9] but in two spatial dimensions typically incur a factorization cost scaling as $\mathcal{O}(N^{3/2})$, where N is the number of unknowns [16, 13]. Krylov subspace methods can achieve near-linear complexity when paired with effective preconditioners, yet the design of robust preconditioners for highly heterogeneous or anisotropic coefficients remains challenging [3, 17, 19]. Multigrid and domain decomposition methods [5, 6, 25] require the careful construction of smoothers, transfer operators, and coarse spaces, and their convergence may deteriorate in the presence of complex coefficient variations [29, 28].

Spectral methods and global eigenfunction expansions [4, 7] exploit analytic structure of the Laplacian to obtain highly compact solution representations. Classical spectral discretizations build the operator directly in a trigonometric or polynomial basis, producing dense matrices and complicating the treatment of variable coefficients [26]. The approach considered here separates discretization from compression: the elliptic operator is discretized in a standard physical-space basis, while a small number of analytically known Dirichlet Laplacian eigenmodes serves as a global compression transform.

The main idea is to construct a global coarse space spanned by the lowest Laplacian eigenmodes, which capture the large-scale energy distribution of elliptic solutions [1]. The full discrete operator and right-hand side are projected onto this subspace, yielding a reduced

Key words and phrases. Elliptic boundary value problems, model reduction, spectral methods, Laplacian eigenfunctions, Schur complement, numerical linear algebra.

Galerkin system of dimension K , where M is the modal cutoff. The reduced operator retains the complete heterogeneity of the coefficient field through the stiffness matrix, while the spectral basis provides a compact representation of the dominant low-frequency components. Elliptic regularity ensures that discarded high modes contribute only weakly to the solution energy [14, 18], so the reduced solution remains accurate.

This construction differs from multigrid, where coarse spaces arise from geometric coarsening and high frequencies are treated by smoothing [5, 6]; from deflation techniques, which rely on approximations of near-null eigenvectors of the stiffness matrix [22, 27]; and from reduced-basis or POD models, which require parameter sampling and snapshot data [20, 15]. Here the coarse space is analytic, independent of the stiffness matrix, and requires no training. The resulting method is non-iterative: once projected quantities are assembled, only a dense system of size K is solved before lifting the solution back to the full discrete space.

The remainder of the paper is organized as follows. Section 2 introduces the model problem and its variational formulation, together with the standard Galerkin discretization. Section 3 presents the spectral low-mode reduced operator and establishes its basic projection properties. In Section 4, we develop a detailed error analysis, including spectral decay estimates, bounds for the discrete reduced solution, and a Schur complement interpretation of the reduction. Section 5 analyzes the computational complexity of the proposed solver. Numerical experiments demonstrating accuracy, robustness, conditioning behavior, and performance relative to standard solvers are reported in Section 6. Conclusions and perspectives for future work are given in the final section.

2. Model Problem and Variational Formulation

We consider the second-order elliptic boundary value problem

$$(2.1) \quad -\nabla \cdot (\kappa(x) \nabla u(x)) = f(x), \quad x \in \Omega = (0, 1)^2,$$

with homogeneous Dirichlet boundary condition

$$(2.2) \quad u(x) = 0, \quad (x) \in \partial\Omega.$$

The coefficient κ is assumed to satisfy the uniform ellipticity $0 < \kappa_{\min} \leq \kappa(x) \leq \kappa_{\max} < \infty$ for all $x \in \Omega$. Such operators arise, for example, in stationary diffusion, conductivity, and homogenization problems.

To provide a suitable framework for the analysis to follow, define $V := H_0^1(\Omega)$, the Sobolev space consisting of all functions on Ω with square-integrable weak gradients and vanishing trace on $\partial\Omega$. On this space we use the standard energy inner product

$$(u, v)_{H_0^1} = \int_{\Omega} \nabla u \cdot \nabla v \, dx, \quad \|u\|_{H_0^1} = (u, u)_{H_0^1}^{1/2},$$

which is equivalent to the full H^1 norm by the Poincaré inequality. Multiplying (2.1) by $v \in V$ and integrating by parts yields

$$(2.3) \quad \int_{\Omega} \kappa \nabla u \cdot \nabla v \, dx = \int_{\Omega} f v \, dx.$$

Introduce the bilinear form and linear functional

$$(2.4) \quad a(u, v) = \int_{\Omega} \kappa \nabla u \cdot \nabla v \, dx, \quad \ell(v) = \int_{\Omega} f v \, dx.$$

The corresponding weak formulation reads:

Find $u \in H_0^1(\Omega)$ such that

$$(2.5) \quad a(u, v) = \ell(v) \quad \forall v \in H_0^1(\Omega).$$

The ellipticity bounds imply that

$$a(u, u) \geq \kappa_{\min} \|\nabla u\|_{L^2}^2, \quad |a(u, v)| \leq \kappa_{\max} \|\nabla u\|_{L^2} \|\nabla v\|_{L^2},$$

so a is coercive and continuous on V . The Lax–Milgram theorem therefore guarantees existence and uniqueness of a solution $u \in V$ and the stability estimate

$$\|u\|_{H_0^1} \leq \kappa_{\min}^{-1} \|f\|_{H^{-1}(\Omega)}.$$

The variational framework established in (2.5) forms the basis for numerical approximation. Since the exact solution lies in the infinite-dimensional space $V = H_0^1(\Omega)$, numerical computations require restricting the problem to a finite-dimensional conforming subspace $V_h \subset V$. This discretization of the underlying function space leads to the standard Galerkin formulation presented in the next section.

2.1. Galerkin discretization. Let $V_h \subset H_0^1(\Omega)$ be a finite-dimensional subspace. The Galerkin approximation seeks $u_h \in V_h$ such that

$$(2.6) \quad a(u_h, v_h) = \ell(v_h) \quad \forall v_h \in V_h.$$

Choosing a basis $\{\psi_i\}_{i=1}^N$ of V_h and writing $u_h = \sum_{j=1}^N U_j \psi_j$ leads to the matrix system

$$(2.7) \quad AU = F, \quad A_{ij} = a(\psi_i, \psi_j), \quad F_i = \ell(\psi_i),$$

where $A \in \mathbb{R}^{N \times N}$ is symmetric positive definite. The reduced-order scheme below acts on (2.7) by projecting onto a carefully chosen low-dimensional spectral subspace.

3. Spectral Low-Mode Reduced Operator

The reduced operator is obtained by restricting the variational problem to a low-dimensional subspace spanned by Laplacian eigenfunctions. This section introduces the spectral space and the associated reduced Galerkin formulation.

3.1. Laplacian eigenfunctions as a coarse space. The Dirichlet Laplacian $-\Delta$ on $\Omega = (0, 1)^2$ admits the well-known eigenpairs

$$(3.1) \quad \phi_{mn}(x) = \sin(m\pi x) \sin(n\pi y), \quad \lambda_{mn} = \pi^2(m^2 + n^2), \quad m, n \geq 1.$$

The family $\{\phi_{mn}\}_{m,n \geq 1}$ forms an orthogonal basis of $L^2(\Omega)$ with respect to the standard inner product and is orthogonal in $H_0^1(\Omega)$ under the weighted energy inner product in (2.4). The eigenvalues grow quadratically with frequency, so high indices correspond to strongly oscillatory components.

For a fixed cutoff $M \geq 1$ define the index set $\mathcal{I} = \{(m, n) : 1 \leq m, n \leq M\}$ and the corresponding low-mode subspace

$$V_M = \text{span}\{\phi_{mn} : (m, n) \in \mathcal{I}\}, \quad K = \dim(V_M) = M^2.$$

In the procedure discussed, this serves as a global coarse space in which the solution is approximated. The choice of M controls the dimension of the reduced system.

3.2. Reduced variational formulation. Let $V_M \subset H_0^1(\Omega)$ denote the spectral subspace spanned by the first K Dirichlet Laplacian eigenfunctions. Since V_M is not contained in the discrete space V_h , we define the discrete low-mode space $V_M^h := \Pi_h V_M \subset V_h$, where $\Pi_h : H_0^1(\Omega) \rightarrow V_h$ denotes a fixed projection or interpolation operator onto the finite element space. In practice, Π_h is taken as the nodal interpolation operator (or, equivalently, the L^2 or energy projection), applied to each spectral basis function. Let $B \in \mathbb{R}^{N \times K}$ be the matrix whose columns contain the coefficients of the projected spectral basis functions $\{\Pi_h \phi_{mn}\}_{1 \leq m, n \leq M}$ expressed in the finite element basis $\{\psi_i\}_{i=1}^N$ of V_h . The range of B therefore spans V_M^h .

The reduced Galerkin approximation seeks $u_{\text{RD}} \in V_M^h$ satisfying

$$a(u_{\text{RD}}, v_M) = \ell(v_M) \quad \forall v_M \in V_M^h.$$

Representing $u_{\text{RD}} = Bz$ and $v_M = Bw$ with $w, z \in \mathbb{R}^K$ and inserting these expansions into (2.7) yields the reduced linear system

$$(3.2) \quad \mathcal{A}z = f_M,$$

where $\mathcal{A} = B^T AB$, and $f_M = B^T F$. After computing z , the reduced approximation in V_h is reconstructed as

$$(3.3) \quad u_{\text{RD}} = Bz.$$

The matrix \mathcal{A} is precisely the stiffness matrix associated with the restriction of a to V_M^h . In continuous form, its entries satisfy

$$\mathcal{A}_{(pq),(mn)} = \int_{\Omega} \kappa \nabla \phi_{mn} \cdot \nabla \phi_{pq} \, dx,$$

so that the full coefficient κ is preserved by the spectral projection. For the analysis it is convenient to introduce the a -orthogonal projector $\Pi_M : V_h \rightarrow V_M^h$ defined by

$$(3.4) \quad a(\Pi_M v_h, v_M) = a(v_h, v_M) \quad \forall v_M \in V_M^h.$$

The following result summarizes the basic properties of the reduced solution.

THEOREM 3.1. *Let $u_h \in V_h$ be the Galerkin solution of the variational problem. Then u_h admits the orthogonal decomposition $u_h = \Pi_M u_h + (I - \Pi_M) u_h$, where $(I - \Pi_M) u_h$ is a -orthogonal to V_M^h . Moreover, the reduced solution $u_{\text{RD}} \in V_M^h$ obtained from the reduced variational problem*

$$a(u_{\text{RD}}, v_M) = \ell(v_M) \quad \forall v_M \in V_M^h$$

coincides with the projection $u_{\text{RD}} = \Pi_M u_h$ and satisfies the best-approximation property

$$\|u_h - u_{\text{RD}}\|_a = \min_{v_M \in V_M^h} \|u_h - v_M\|_a, \quad \|w\|_a^2 := a(w, w).$$

PROOF. Since a is continuous and coercive on V_h , the projection Π_M is well defined. Then

$$a(u_h - \Pi_M u_h, v_M) = 0 \quad \forall v_M \in V_M^h,$$

which yields the orthogonal decomposition $u_h = \Pi_M u_h + (I - \Pi_M) u_h$. The reduced solution $u_{\text{RD}} \in V_M^h$ satisfies

$$a(u_{\text{RD}}, v_M) = \ell(v_M) \quad \forall v_M \in V_M^h.$$

Since u_h satisfies $a(u_h, v_M) = \ell(v_M)$ for all $v_M \in V_M^h$, subtracting the two equalities gives

$$a(u_h - u_{\text{RD}}, v_M) = 0 \quad \forall v_M \in V_M^h.$$

Thus u_{RD} is the unique element of V_M^h that is a -orthogonal to $u_h - u_{\text{RD}}$, which is exactly the defining property of the a -orthogonal projection. Hence $u_{\text{RD}} = \Pi_M u_h$.

The best-approximation property follows from orthogonality: for any $v_M \in V_M^h$,

$$\|u_h - u_{\text{RD}}\|_a^2 \leq a(u_h - v_M, u_h - v_M) = \|u_h - v_M\|_a^2.$$

Taking the minimum over all $v_M \in V_M^h$ yields the stated result. \square

This result shows that u_{RD} is the energy-optimal approximation to u_h in V_M^h , and that the error $u_h - u_{\text{RD}}$ is exactly the high-frequency component of u_h lying in the orthogonal complement $V_M^{h \perp}$. To evaluate the accuracy of the reduced approximation, we quantify the effect of projection onto V_M^h and the role of the discarded high modes. The next section develops these estimates, establishing spectral decay of the solution, the energy-optimality of the projection, and bounds for both the discretization and reduction errors.

4. Error Analysis

The error analysis relies on the decay of Laplacian eigen-coefficients for elliptic solutions and on the projection structure in Theorem 3.1. The goal is to relate the reduced-order error to the regularity of the continuous solution and the spectral cutoff M .

4.1. Spectral decay and continuous projection. For smooth coefficients and data, elliptic regularity implies H^2 -regularity of the solution and, consequently, quantitative decay of its Laplace eigen-expansion. The next result states a convenient form of this decay and the resulting projection error.

THEOREM 4.1. *Let $\Omega = (0, 1)^2$ and let $\{(\phi_{m,n}, \lambda_{m,n})\}_{m,n \geq 1}$ denote the $L^2(\Omega)$ -orthonormal Dirichlet eigenpairs of $-\Delta$, with $\lambda_{m,n} = \pi^2(m^2 + n^2)$. Assume $u \in H^2(\Omega) \cap H_0^1(\Omega)$ and write $u = \sum_{m,n \geq 1} \hat{u}_{m,n} \phi_{m,n}$. For $M \geq 1$, define the rectangular spectral projector*

$$\Pi_M u := \sum_{1 \leq m \leq M} \sum_{1 \leq n \leq M} \hat{u}_{m,n} \phi_{m,n}.$$

Then there exists a constant $C > 0$, independent of M , such that

$$\|u - \Pi_M u\|_{H_0^1(\Omega)} \leq C \frac{\sqrt{\log M}}{M} \|u\|_{H^2(\Omega)}.$$

PROOF. Using the spectral representation of the H_0^1 seminorm,

$$\|u - \Pi_M u\|_{H_0^1}^2 = \sum_{\substack{m > M \\ \text{or } n > M}} \lambda_{m,n} |\hat{u}_{m,n}|^2 = \sum_{\substack{m > M \\ \text{or } n > M}} \frac{1}{\lambda_{m,n}^2} (\lambda_{m,n}^3 |\hat{u}_{m,n}|^2).$$

Since $u \in H^2(\Omega)$, the spectral characterization of Sobolev norms yields

$$(4.1) \quad \sum_{m,n \geq 1} \lambda_{m,n}^2 |\hat{u}_{m,n}|^2 \lesssim \|u\|_{H^2(\Omega)}^2.$$

Moreover, because $\lambda_{m,n} = \pi^2(m^2 + n^2)$, we have $\lambda_{m,n}^3 |\hat{u}_{m,n}|^2 = \lambda_{m,n} (\lambda_{m,n}^2 |\hat{u}_{m,n}|^2) \lesssim \lambda_{m,n}^2 |\hat{u}_{m,n}|^2$ up to a harmless constant on Ω , so it suffices to estimate the tail weight

$$(4.2) \quad W_M := \sum_{\substack{m > M \\ \text{or } n > M}} \frac{1}{\lambda_{m,n}^2} \sim \sum_{\substack{m > M \\ \text{or } n > M}} \frac{1}{(m^2 + n^2)^2}.$$

Geometrically, the tail index set $T_M := \{(m, n) \in \mathbb{N}^2 : m > M \text{ or } n > M\}$ is the union of two semi-infinite strips. By symmetry,

$$W_M \leq \frac{2}{\pi^4} \sum_{m=M+1}^{\infty} \sum_{n=1}^{\infty} \frac{1}{(m^2 + n^2)^2}.$$

For fixed $m \geq 1$, apply the integral test to the inner sum:

$$\sum_{n=1}^{\infty} \frac{1}{(m^2 + n^2)^2} \leq \int_0^{\infty} \frac{1}{(m^2 + y^2)^2} dy = \frac{\pi}{4m^3}.$$

This bound would yield $W_M \lesssim \sum_{m > M} m^{-3} \lesssim M^{-2}$, which is not sharp for a rectangular tail. To capture the logarithmic factor, split the inner sum at $n = m$:

$$\sum_{n=1}^{\infty} \frac{1}{(m^2 + n^2)^2} = \sum_{n=1}^m \frac{1}{(m^2 + n^2)^2} + \sum_{n=m+1}^{\infty} \frac{1}{(m^2 + n^2)^2}.$$

For $1 \leq n \leq m$, we have $m^2 + n^2 \geq m^2$, hence

$$\sum_{n=1}^m \frac{1}{(m^2 + n^2)^2} \leq \sum_{n=1}^m \frac{1}{m^4} = \frac{1}{m^3}.$$

For $n \geq m + 1$, we have $m^2 + n^2 \geq n^2$, hence

$$\sum_{n=m+1}^{\infty} \frac{1}{(m^2 + n^2)^2} \leq \sum_{n=m+1}^{\infty} \frac{1}{n^4} \lesssim \frac{1}{m^3}.$$

Therefore $\sum_{n=1}^{\infty} (m^2 + n^2)^{-2} \lesssim m^{-3}$, and the strip estimate alone gives $W_M \lesssim M^{-2}$. To obtain the correct $\log M$ behavior for the *union of strips* tail, we instead estimate W_M directly by separating the tail into the two strips and subtracting the overlap:

$$W_M \leq \frac{1}{\pi^4} \left(\sum_{m=M+1}^{\infty} \sum_{n=1}^{\infty} \frac{1}{(m^2 + n^2)^2} + \sum_{n=M+1}^{\infty} \sum_{m=1}^{\infty} \frac{1}{(m^2 + n^2)^2} \right) = \frac{2}{\pi^4} \sum_{m=M+1}^{\infty} \sum_{n=1}^{\infty} \frac{1}{(m^2 + n^2)^2}.$$

Now use the crude but sharp-enough lower bound $(m^2 + n^2) \geq m^2$ to write

$$\frac{1}{(m^2 + n^2)^2} = \frac{1}{m^2 + n^2} \cdot \frac{1}{m^2 + n^2} \leq \frac{1}{m^2} \cdot \frac{1}{m^2 + n^2}.$$

Thus

$$W_M \leq \frac{2}{\pi^4} \sum_{m=M+1}^{\infty} \frac{1}{m^2} \sum_{n=1}^{\infty} \frac{1}{m^2 + n^2}.$$

Using

$$\sum_{n=1}^{\infty} \frac{1}{m^2 + n^2} \leq \int_0^{\infty} \frac{1}{m^2 + y^2} dy = \frac{\pi}{2m},$$

we have

$$W_M \leq C \sum_{m=M+1}^{\infty} \frac{1}{m^3} \leq \frac{C}{M^2}.$$

Finally, on T_M we have $m^2 + n^2 \geq M^2$, so a refinement gives

$$\frac{1}{(m^2 + n^2)^2} \leq \frac{1}{M^2} \cdot \frac{1}{m^2 + n^2},$$

and therefore

$$W_M \leq \frac{C}{M^2} \sum_{\substack{m > M \\ \text{or } n > M}} \frac{1}{m^2 + n^2} \lesssim \frac{\log M}{M^2},$$

where the last estimate follows from the comparison of with $\int_M^{\infty} \int_1^{\infty} (x^2 + y^2)^{-1} dA \sim \log M$. Combining the bound $W_M \lesssim (\log M)/M^2$ with (4.1) and applying Cauchy–Schwarz yields

$$\|u - \Pi_M u\|_{H_0^1}^2 \lesssim \frac{\log M}{M^2} \|u\|_{H^2(\Omega)}^2,$$

which gives the stated estimate after taking square roots. \square

4.2. Error for discrete reduced solution. We now bound the error between the full Galerkin solution u_h and the reduced solution u_{RD} , combining the continuous spectral truncation estimate with standard discretization error bounds.

THEOREM 4.2. *Let u , u_h , and u_{RD} denote the continuous solution, the Galerkin solution, and the reduced solution, respectively. Assume that the finite element discretization satisfies*

$$\|u - u_h\|_{H_0^1} \leq C h \|u\|_{H^2(\Omega)},$$

and that the assumptions of Theorem 4.1 hold. Then there exists a constant $C > 0$, independent of h and M , such that

$$\|u_h - u_{\text{RD}}\|_{H_0^1} \leq C \left(h + \frac{\sqrt{\log M}}{M} \right) \|u\|_{H^2(\Omega)}.$$

Moreover,

$$\|u_h - u_{\text{RD}}\|_{L^2} \leq C \left(h^2 + \frac{1}{\sqrt{\lambda_{M+1,M+1}}} \frac{\sqrt{\log M}}{M} \right) \|u\|_{H^2(\Omega)}.$$

PROOF. By Theorem 3.1, $u_{RD} = \Pi_M u_h$, and hence $u_h - u_{RD} = u_h - \Pi_M u_h$. Inserting u and $\Pi_M u$ yields the decomposition

$$u_h - u_{RD} = (u_h - u) + (u - \Pi_M u) + \Pi_M(u - u_h).$$

Applying the triangle inequality in $H_0^1(\Omega)$ gives

$$(4.3) \quad \|u_h - u_{RD}\|_{H_0^1} \leq \|u - \Pi_M u\|_{H_0^1} + \|u - u_h\|_{H_0^1} + \|\Pi_M(u - u_h)\|_{H_0^1}.$$

The first term is bounded by Theorem 4.1:

$$\|u - \Pi_M u\|_{H_0^1} \leq C \frac{\sqrt{\log M}}{M} \|u\|_{H^2(\Omega)}.$$

Since Π_M is an a -orthogonal projector and a is coercive and continuous on V_h , there exists $C > 0$ such that $\|\Pi_M v_h\|_{H_0^1} \leq C \|v_h\|_{H_0^1}$ for all $v_h \in V_h$. Therefore,

$$\|\Pi_M(u - u_h)\|_{H_0^1} \leq C \|u - u_h\|_{H_0^1} \leq C h \|u\|_{H^2(\Omega)}.$$

Substituting these bounds into (4.3) yields

$$\|u_h - u_{RD}\|_{H_0^1} \leq C \left(h + \frac{\sqrt{\log M}}{M} \right) \|u\|_{H^2(\Omega)},$$

which proves the H_0^1 estimate.

For the L^2 estimate, write $u - u_{RD} = (u - \Pi_M u) + \Pi_M(u - u_h)$, so that

$$(4.4) \quad \|u - u_{RD}\|_{L^2} \leq \|u - \Pi_M u\|_{L^2} + \|\Pi_M(u - u_h)\|_{L^2}.$$

The first term contains only high Laplacian modes. Using $\lambda_{m,n} \geq \lambda_{M+1,M+1}$ on the tail,

$$\|u - \Pi_M u\|_{L^2}^2 = \sum_{\substack{m > M \\ \text{or } n > M}} |\hat{u}_{m,n}|^2 \leq \frac{1}{\lambda_{M+1,M+1}} \sum_{\substack{m > M \\ \text{or } n > M}} \lambda_{m,n} |\hat{u}_{m,n}|^2 = \frac{1}{\lambda_{M+1,M+1}} \|u - \Pi_M u\|_{H_0^1}^2.$$

Applying Theorem 4.1 gives

$$\|u - \Pi_M u\|_{L^2} \leq C \lambda_{M+1,M+1}^{-1/2} \frac{\sqrt{\log M}}{M} \|u\|_{H^2(\Omega)}.$$

For the second term in (4.4), the projector Π_M is L^2 -stable, hence

$$\|\Pi_M(u - u_h)\|_{L^2} \leq \|u - u_h\|_{L^2} \leq C h^2 \|u\|_{H^2(\Omega)}.$$

Combining these estimates yields

$$\|u - u_{RD}\|_{L^2} \leq C \left(h^2 + \lambda_{M+1,M+1}^{-1/2} \frac{\sqrt{\log M}}{M} \right) \|u\|_{H^2(\Omega)}.$$

Finally, using $u_h - u_{RD} = (u_h - u) + (u - u_{RD})$ and the finite-element L^2 estimate for $\|u - u_h\|_{L^2}$ gives the stated bound for $\|u_h - u_{RD}\|_{L^2}$. \square

4.3. Convergence of the reduced method. The total error of the spectral low-mode approximation consists of the discretization error associated with the Galerkin solution u_h and the additional projection error introduced by restricting the approximation to the reduced space V_M^h . For the underlying finite-difference or finite-element discretization one has the classical estimates

$$\|u - u_h\|_{H_0^1} = \mathcal{O}(h), \quad \|u - u_h\|_{L^2} = \mathcal{O}(h^2),$$

while Theorem 4.2 shows that the reduced solution satisfies

$$\|u_h - u_{RD}\|_{H_0^1} = \mathcal{O}\left(h + \frac{\sqrt{\log M}}{M}\right), \quad \|u_h - u_{RD}\|_{L^2} = \mathcal{O}\left(h^2 + \lambda_{M+1,M+1}^{-1/2} \frac{\sqrt{\log M}}{M}\right).$$

Combining these bounds yields

$$\|u - u_{RD}\|_{H_0^1} \lesssim h + \frac{\sqrt{\log M}}{M}, \quad \|u - u_{RD}\|_{L^2} \lesssim h^2 + \lambda_{M+1,M+1}^{-1/2} \frac{\sqrt{\log M}}{M},$$

with constants independent of h and M . The contribution of the discarded high modes therefore remains negligible provided the cutoff grows with refinement so that $\sqrt{\log M}/M \lesssim h$. Since $\lambda_{M+1,M+1} \sim (M+1)^2$, this condition implies that the projection term in the L^2 estimate is also $O(h^2)$. Under this scaling, the reduced solution inherits the same convergence rates as the full discretization,

$$\|u - u_{\text{RD}}\|_{H_0^1} = \mathcal{O}(h), \quad \|u - u_{\text{RD}}\|_{L^2} = \mathcal{O}(h^2),$$

and the spectral reduction does not degrade the accuracy of the underlying scheme.

4.4. High–low coupling and Schur complement truncation. The reduced operator may be interpreted as the leading term in a Schur complement representation of the full discrete operator. This viewpoint clarifies the effect of discarding high–frequency interactions and provides a natural framework for quantifying the resulting approximation error. Let $V = V_M \oplus V_H$ denote the H_0^1 –orthogonal decomposition, where $V_H = V_M^\perp$. With respect to this splitting, the operator A associated with the bilinear form a admits the block representation

$$A = \begin{pmatrix} A_{LL} & A_{LH} \\ A_{HL} & A_{HH} \end{pmatrix},$$

where $A_{LL} : V_M \rightarrow V_M'$, $A_{HH} : V_H \rightarrow V_H'$, and $A_{LH} : V_H \rightarrow V_M'$ denote the coarse, fine, and coupling components, respectively. Eliminating the high–frequency variables yields the exact Schur complement $S = A_{LL} - A_{LH}A_{HH}^{-1}A_{HL}$.

The spectral reduced method replaces the exact Schur complement S by its leading block A_{LL} , thereby neglecting the correction term $A_{LH}A_{HH}^{-1}A_{HL}$. This truncation may be viewed as neglecting a spectrally small correction that quantifies the interaction between retained low modes and eliminated high modes; its size is controlled by decay of the coupling block A_{LH} with the spectral cutoff, as established in Theorem 4.3. The following result provides a bound on the resulting truncation error in terms of the regularity of the coefficient field.

THEOREM 4.3. *Let $\kappa(x) = \kappa_0 + \tilde{\kappa}(x)$ with $\kappa_0 = |\Omega|^{-1} \int_{\Omega} \kappa \, dx$ and $\tilde{\kappa} \in H^s(\Omega)$ for some $s > 1$ satisfying $\int_{\Omega} \tilde{\kappa} \, dx = 0$. Assume $0 < \kappa_{\min} \leq \kappa \leq \kappa_{\max}$ on Ω . Let V_M be the subspace spanned by the first K Dirichlet Laplacian eigenfunctions and $V_H = V_M^\perp$ in $H_0^1(\Omega)$. Then there exists $C = C(\Omega, s) > 0$ such that for all $u_L \in V_M$ and $u_H \in V_H$,*

$$(4.5) \quad |a(u_L, u_H)| \leq C \lambda_{M+1,M+1}^{-(s-1)/2} \|\tilde{\kappa}\|_{H^s(\Omega)} \|u_L\|_{H_0^1} \|u_H\|_{H_0^1},$$

where $\lambda_{M+1,M+1}$ is the $(M+1, M+1)$ Dirichlet Laplacian eigenvalue. In particular,

$$(4.6) \quad \|A_{LH}\|_{\mathcal{I}(V_M, V_H)} \leq C \lambda_{M+1,M+1}^{-(s-1)/2} \|\tilde{\kappa}\|_{H^s(\Omega)}.$$

PROOF. Since V_M and V_H are H_0^1 –orthogonal, $\int_{\Omega} \kappa_0 \nabla u_L \cdot \nabla u_H \, dx = 0$, and it follows from the decomposition of κ that

$$a(u_L, u_H) = \int_{\Omega} \tilde{\kappa} \nabla u_L \cdot \nabla u_H \, dx.$$

Let $\{\phi_k\}$ be the Laplacian eigenfunctions with eigenvalues $\{\lambda_k\}$, and set $e_k = \lambda_k^{-1/2} \phi_k$, forming an H_0^1 –orthonormal basis. Expanding $u_L = \sum_{i \leq K} \hat{u}_i e_i$ and $u_H = \sum_{j > K} \hat{u}_j e_j$, gives

$$a(u_L, u_H) = \sum_{i \leq K} \sum_{j > K} \hat{u}_i \hat{u}_j M_{ij}, \quad M_{ij} = \int_{\Omega} \tilde{\kappa} \nabla e_i \cdot \nabla e_j \, dx.$$

Using $e_k = \lambda_k^{-1/2} \phi_k$ and integrating by parts, one obtains

$$\nabla e_i \cdot \nabla e_j = \lambda_i^{1/2} \lambda_j^{1/2} \phi_i \phi_j - \lambda_i^{-1/2} \lambda_j^{-1/2} \nabla \tilde{\kappa} \cdot (\phi_j \nabla \phi_i).$$

Thus, an explicit expression for M_{ij} is

$$M_{ij} = \lambda_i^{1/2} \lambda_j^{1/2} \int_{\Omega} \tilde{\kappa} \phi_i \phi_j \, dx - \lambda_i^{-1/2} \lambda_j^{-1/2} \int_{\Omega} \phi_j \nabla \tilde{\kappa} \cdot \nabla \phi_i \, dx.$$

Since $\tilde{\kappa} \in H^s(\Omega)$ with $s > 1$, the spectral Sobolev characterization implies

$$\|\phi_k\|_{H^s} \sim \lambda_k^{s/2}, \quad \|\nabla \phi_k\|_{L^2} \sim \lambda_k^{1/2},$$

and therefore each term in M_{ij} satisfies

$$|M_{ij}| \leq C \|\tilde{\kappa}\|_{H^s(\Omega)} \lambda_{\max\{i,j\}}^{-(s-1)/2}.$$

For $i \leq K$ and $j > K$, this gives

$$|M_{ij}| \leq C \|\tilde{\kappa}\|_{H^s(\Omega)} \lambda_{M+1,M+1}^{-(s-1)/2}.$$

Using Cauchy–Schwarz and the orthonormality of $\{e_k\}$,

$$|a(u_L, u_H)| \leq \sup_{i \leq K, j > K} |M_{ij}| \left(\sum_{i \leq K} |\hat{u}_i|^2 \right)^{1/2} \left(\sum_{j > K} |\hat{u}_j|^2 \right)^{1/2} = \sup_{i \leq K, j > K} |M_{ij}| \|u_L\|_{H_0^1} \|u_H\|_{H_0^1},$$

which proves (4.5). Taking the supremum over nonzero pairs (u_L, u_H) yields (4.6). \square

Combining (4.6) with a Schur complement estimate yields a bound for the difference between the exact coarse operator S and A_{LL} .

THEOREM 4.4. *Assume A_{HH} is coercive on V_H with constant $\alpha_H > 0$, so that*

$$a(w_H, w_H) \geq \alpha_H \|w_H\|_{H_0^1}^2 \quad \forall w_H \in V_H.$$

Let $S = A_{LL} - A_{LH}A_{HH}^{-1}A_{HL}$ be the Schur complement. Then

$$\|S - A_{LL}\|_{\mathcal{I}(V_M, V'_M)} \leq \frac{1}{\alpha_H} \|A_{LH}\|_{\mathcal{I}(V_M, V_H)}^2.$$

In particular, with (4.6),

$$\|S - A_{LL}\|_{\mathcal{I}(V_M, V'_M)} \lesssim \frac{\|\tilde{\kappa}\|_{H^s(\Omega)}^2}{\alpha_H} \lambda_{M+1,M+1}^{-(s-1)}.$$

PROOF. By the definition of S , we have $S - A_{LL} = -A_{LH}A_{HH}^{-1}A_{HL}$, and therefore

$$\|S - A_{LL}\| \leq \|A_{LH}\| \|A_{HH}^{-1}\| \|A_{HL}\|.$$

Since $A_{HL} = A_{LH}^*$, it follows that $\|A_{HL}\| = \|A_{LH}\|$. From the coercivity of A_{HH} , it also implies $\|A_{HH}^{-1}\| \leq 1/\alpha_H$ in the natural norms, whence

$$\|S - A_{LL}\| \leq \frac{1}{\alpha_H} \|A_{LH}\|^2.$$

The last estimate follows by substituting (4.6). \square

The stability properties of the reduced operator imply that its spectrum remains bounded away from zero and infinity when restricted to the spectral subspace. To make this observation precise, it is useful to examine the conditioning of its matrix representation. Since the reduced space has fixed dimension K , one expects the conditioning of the projected operator to be governed solely by the continuity and coercivity constants of the underlying bilinear form, independent of both the mesh size and (for uniformly stable bases) the choice of the modal cutoff. The next result formalizes this observation.

THEOREM 4.5. *Let a be the bilinear form defined in (2.4), assumed continuous and coercive on $V = H_0^1(\Omega)$. Let $V_M^h \subset V_h \subset V$ be the discrete spectral subspace and $A_{LL} \in \mathbb{R}^{K \times K}$ the reduced stiffness matrix associated with a on V_M^h , written in a basis $\{\psi_i\}_{i=1}^K$ of V_M^h whose H_0^1 Gram matrix $G_{ij} = (\psi_j, \psi_i)_{H_0^1}$ is uniformly well conditioned with respect to h and M . If*

$$(A_{LL})_{ij} = a(\psi_j, \psi_i),$$

then A_{LL} is symmetric positive definite and there exists a constant $C_{\text{cond}} > 0$, independent of h and M , such that

$$\kappa_2(A_{LL}) = \frac{\lambda_{\max}(A_{LL})}{\lambda_{\min}(A_{LL})} \leq C_{\text{cond}}.$$

In particular, C_{cond} depends on the continuity and coercivity constants and on the basis stability through $\kappa_2(G)$.

PROOF. Let $\{\psi_i\}_{i=1}^K$ be a basis of V_M^h and $A_{LL} \in \mathbb{R}^{K \times K}$ be defined by $(A_{LL})_{ij} = a(\psi_j, \psi_i)$. For any coefficient vector $x = (x_1, \dots, x_K)^T \in \mathbb{R}^K$ define $v_M = \sum_{i=1}^K x_i \psi_i \in V_M^h$. Then

$$x^T A_{LL} x = a(v_M, v_M).$$

By coercivity and continuity of a on V ,

$$\alpha_a \|v_M\|_{H_0^1}^2 \leq a(v_M, v_M) \leq C_a \|v_M\|_{H_0^1}^2 \quad \forall v_M \in V_M^h.$$

Let $G \in \mathbb{R}^{K \times K}$ be such that $G_{ij} = (\psi_j, \psi_i)_{H_0^1}$. Then

$$\|v_M\|_{H_0^1}^2 = x^T G x.$$

Hence, for all $x \in \mathbb{R}^K$,

$$\alpha_a x^T G x \leq x^T A_{LL} x \leq C_a x^T G x.$$

Let λ_{\min} and λ_{\max} denote the smallest and largest eigenvalues of a symmetric positive definite matrix. The Rayleigh quotient characterization implies

$$\alpha_a \lambda_{\min}(G) \leq \lambda_{\min}(A_{LL}) \leq \lambda_{\max}(A_{LL}) \leq C_a \lambda_{\max}(G).$$

Therefore

$$\kappa_2(A_{LL}) = \frac{\lambda_{\max}(A_{LL})}{\lambda_{\min}(A_{LL})} \leq \frac{C_a}{\alpha_a} \frac{\lambda_{\max}(G)}{\lambda_{\min}(G)} = \frac{C_a}{\alpha_a} \kappa_2(G).$$

The Gram matrix G depends only on the choice of basis in V_M^h ; for any uniformly stable choice of basis the condition number $\kappa_2(G)$ is bounded independently of h and M . Thus

$$\kappa_2(A_{LL}) \leq C_{\text{cond}} := \frac{C_a}{\alpha_a} \sup_{h,M} \kappa_2(G),$$

which is finite and independent of N and K . This proves the claim. \square

5. Complexity Analysis

The spectral reduction procedure replaces the full discrete Galerkin system of dimension $N = \dim(V_h)$ by a projected system of dimension $K = \dim(V_M^h) = M^2$. Its computational cost is governed by the formation of the reduced operator $A_{LL} = B^T A B$, the reduced load vector $f_M = B^T F$, and the solution of the resulting dense $K \times K$ system. Since the stiffness matrix A in two dimensions contains $\mathcal{O}(N)$ nonzero entries, multiplication of A by the matrix $B \in \mathbb{R}^{N \times K}$ costs $\mathcal{O}(NK)$ floating-point operations when B is applied as a dense matrix (as in the implementation reported here). Left multiplication by B^T to assemble A_{LL} and f_M incurs an additional $\mathcal{O}(NK)$ operations. Thus the cost of forming the reduced system is $\mathcal{O}(NK)$.

The matrix A_{LL} is dense and of fixed size $K \times K$. Solving the system $A_{LL}z = f_M$ by Gaussian elimination or Cholesky factorization requires $\mathcal{O}(K^3)$ operations. Combining this with the assembly cost yields the overall complexity

$$\mathcal{C}_{\text{RD}} = \mathcal{O}(NK) + \mathcal{O}(K^3).$$

When K is chosen independently of N —as is typical when M is held moderate—the term $\mathcal{O}(K^3)$ is constant and the cost of the entire reduced solver is linear in N (for fixed K). This should be compared with the cost of solving the full system $AU = F$ by sparse Cholesky factorization. For a quasi-uniform mesh in two dimensions, the elimination graph exhibits fill-in on the order of $N^{1/2}$, leading to a factorization cost of $\mathcal{O}(N^{3/2})$. Since $N^{3/2}$ grows strictly faster than N , the spectral reduced solver becomes asymptotically more efficient than sparse direct methods whenever K remains bounded as the mesh is refined. This difference in scaling is reflected in the numerical experiments, where the reduced solver exhibits essentially linear growth in runtime with the number of degrees of freedom for fixed K .

6. Numerical Experiments

This section reports numerical experiments designed to assess the accuracy and performance of the spectral low-mode reduced method. The goals are to confirm the error estimates of Section 4, to examine the effect of the spectral cutoff M on the approximation, and to compare the cost of the reduced solver with that of solving the full discrete system. In this setting, the standard five-point finite difference discretization attains the same second-order accuracy as conforming finite elements and avoids the additional overhead associated with quadrature and element assembly. The Cartesian grid also aligns naturally with the Laplace eigenmodes that span the reduced space and permits direct evaluation at grid nodes and simplifying the construction of the projected operator.

6.1. Example 1. We consider (2.1)–(2.2) with manufactured solution $u = \sin(\pi x) \sin(\pi y)$ and diffusion coefficient $\kappa = 1 + \frac{1}{2} \sin(2\pi x) \sin(2\pi y)$. The corresponding forcing term is obtained by substituting u and κ into (2.1). The reduced method is tested in terms of accuracy and computational performance relative to the finite difference discretization.

6.1.1. Performance. We first assess the accuracy and computational efficiency of the spectral low-mode reduced solver relative to the finite difference (FD) discretization. Table 1 reports the L_2 errors of both methods together with the observed speed-up obtained by the reduced solver across a sequence of grid resolutions.

N_x	L_2 -Error		
	FD	Reduced	Speed-up
128	2.4872×10^{-5}	2.4905×10^{-5}	2.431
256	6.2656×10^{-6}	6.2740×10^{-6}	3.044
512	1.5724×10^{-6}	1.5746×10^{-6}	3.651
1024	3.9387×10^{-7}	3.9440×10^{-7}	4.446
2048	9.8564×10^{-8}	9.8697×10^{-8}	4.932

TABLE 1. L_2 errors and computational speed-up for the finite difference and spectral reduced solvers.

The errors produced by the two approaches agree to within a few parts in 10^3 for all grid sizes, indicating that the reduction error introduced by the spectral projection is negligible compared to the underlying discretization error. This observation is consistent with the error estimates of Section 4, which predict that the contribution of discarded high-frequency modes is asymptotically small. The convergence behavior is further illustrated in Figure 1, which displays the L_2 error as a function of grid spacing.

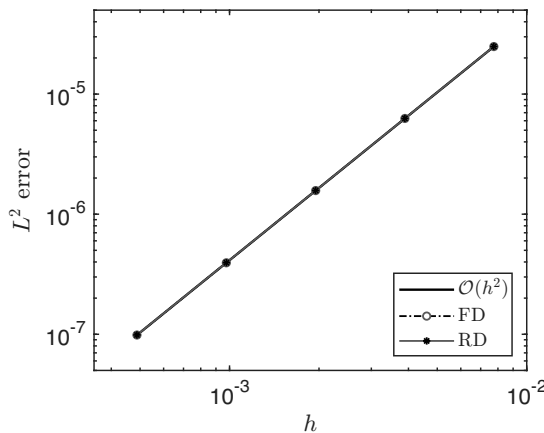


FIGURE 1. L^2 -error convergence for the finite difference and spectral reduced solvers.

Both methods exhibit second-order convergence, matching the accuracy of the underlying finite difference scheme. From a computational standpoint, the reduced solver achieves speed-up factors ranging from approximately 2.4 to 5 as the grid is refined. This gain reflects the essentially linear complexity of the projection-based reduced solve, in contrast to the superlinear scaling of the sparse direct solver applied to the full system.

6.1.2. Convergence. While the results above demonstrate that a fixed spectral cutoff reproduces the accuracy of the full discretization, it is also of interest to examine the dependence of the reduced approximation on the dimension of the spectral space. With the projection estimate $C\sqrt{\log M}/M$ in mind, we next study the effect of varying the cutoff M . To isolate this effect from discretization errors, we fix a fine grid with $m = 1024$ and report the L_2 error as a function of K .

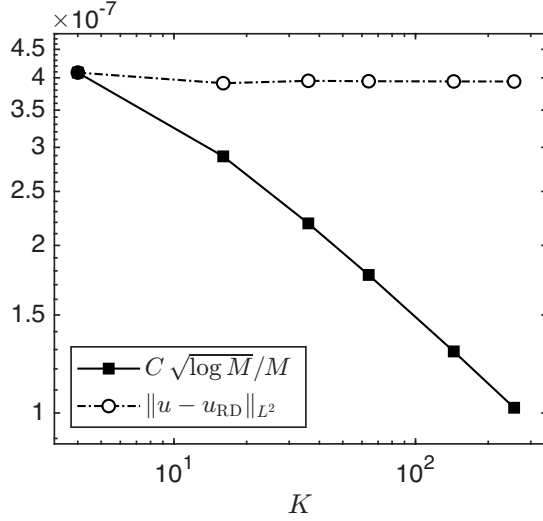


FIGURE 2. L_2 error of the reduced solution versus spectral dimension K on the fixed grid $m = 1024$.

In the reference curve $C\sqrt{\log M}/M$, the constant C is chosen by normalizing the bound at the smallest spectral cutoff M_1 used in the experiment, namely

$$C = \frac{\|u - u_{RD}^{(M_1)}\|_{L^2}}{\sqrt{\log M_1}/M_1}.$$

This choice removes the unknown prefactor in the asymptotic estimate and allows the comparison to emphasize the predicted decay rate with respect to the spectral cutoff M . From the theoretical estimate of Theorem 4.1, the constant C is proportional to $\|u\|_{H^2(\Omega)}$, but since this quantity is not directly available in discrete computations, the normalization above provides a practical surrogate for visualizing the asymptotic behavior.

As shown in Figure 2, the L_2 error decreases slightly as M increases from 2 to 4, and then remains essentially unchanged for larger values of M . This saturation indicates that for $M \geq 4$ the projection error is already dominated by the underlying finite difference error. Consequently, additional spectral modes do not yield any noticeable improvement in accuracy. In particular, choices such as $M = 8$ or $M = 16$ provide full fine-grid accuracy while retaining a reduced space dimension $K \ll N$. To separate the influence of the spectral cutoff from the discretization error more clearly, we also compute the reduction error $\|u_{FD} - u_{RD}\|_{L^2}$ for varying values of M .

Figure 3 shows a rapid decay of the reduction error as additional low-frequency modes are included. Increasing the cutoff from $M = 2$ to $M = 4$ reduces the error by nearly an order of magnitude, and the error continues to decrease steadily for larger values of M . Already at $M = 8$, the reduction error falls below 10^{-8} , while further increases in M produce only modest improvements. This behavior is consistent with the diminishing returns predicted by

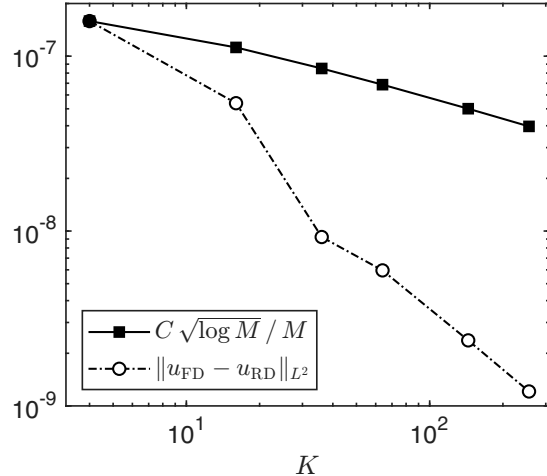


FIGURE 3. Reduction error $\|u_{\text{FD}} - u_{\text{RD}}\|_{L^2}$ versus spectral cutoff M on the fixed grid $m = 1024$.

the estimate $\sqrt{\log M}/M$ and confirms that a very small spectral subspace suffices to recover the full finite difference solution on a fine grid.

6.2. Example 2. We consider (2.1)–(2.2) with manufactured solution $u(x) = \sin(\pi x) \sin(\pi y)$, and the highly oscillatory coefficient $\kappa = 1 + 0.9 \sin(8\pi x) \sin(8\pi y)$.

6.2.1. Robustness. Table 2 reports the L_2 errors and computational speed-up for both the full FD solution and the Reduced solution on grids ranging from 128^2 to 2048^2 interior points.

N_x	L_2 -Error		
	FD	Reduced	Speed-up
128	3.6863×10^{-4}	1.3466×10^{-4}	2.289
256	9.3492×10^{-5}	3.3966×10^{-5}	3.250
512	2.3504×10^{-5}	8.5269×10^{-6}	3.546
1024	5.8898×10^{-6}	2.1360×10^{-6}	4.097
2048	1.4741×10^{-6}	5.3454×10^{-7}	4.499

TABLE 2. L_2 errors and speed-up for the spectral reduced solver with oscillatory diffusion coefficient.

Although both methods exhibit the same second-order convergence rate, the reduced approximation consistently attains a smaller error constant. This behavior is expected, since the reduced solution is obtained from a global Galerkin projection onto a smooth spectral subspace, which can reduce the error constant relative to a local finite difference discretization without altering the asymptotic order. The accuracy of the reduced approximation is maintained even though the spectral space dimension is fixed ($K = 64$), indicating that the dominant solution components are captured by a small number of global modes. These results confirm that the method remains effective for rapidly varying coefficients and does not depend on slow spatial variation of the diffusion field.

6.2.2. Comparison with Direct, Multigrid, and Deflation Methods. To complement the accuracy of the results above and place the reduced solver in a broader context, we examine its computational performance relative to standard solvers commonly used for elliptic problems. In particular, we compare wall-clock runtimes against a sparse direct solver, a geometric multigrid (GMG)-preconditioned Krylov method, and a deflation-based Krylov method. This comparison highlights differences in scalability, robustness, and setup cost that are not visible from error metrics alone. Table 3 shows that the spectral reduced solver exhibits consistently favorable performance across all tested grid sizes. While the sparse direct solver is competitive

on the coarsest grids, its runtime increases rapidly as the number of unknowns grows, reflecting the expected superlinear complexity of sparse factorization in two dimensions.

m	$N = m^2$	Direct	Reduced	GMG	GMG it.	Defl. it.
32	1024	0.001	0.002	0.091	281	9
64	4096	0.004	0.003	0.058	188	15
128	16384	0.011	0.006	0.204	241	19
256	65536	0.045	0.020	0.961	239	32

TABLE 3. Runtimes (in seconds) for the sparse direct solver, the spectral low-mode reduced (Reduced) solver with fixed $M = 8$, and a geometric multigrid (GMG)-preconditioned Krylov solver.

In contrast, the reduced solver shows only mild growth in runtime, consistent with the linear complexity predicted by the projection-based formulation for fixed reduced dimension. The multigrid-preconditioned Krylov solver converges in all cases but requires a large and nonuniform number of iterations, resulting in significantly higher runtimes. This behavior illustrates the sensitivity of multigrid performance to coefficient variability and smoother effectiveness. Deflation reduces iteration counts relative to GMG but incurs additional overhead associated with constructing the deflation space from approximate eigenvectors of the heterogeneous operator. Overall, these results indicate that, in the experiments reported here (for this oscillatory coefficient and with the GMG/deflation implementations and parameters used), the proposed spectral low-mode reduced solver provides a competitive and robust alternative to both direct and iterative methods.

6.2.3. Conditioning sensitivity. To complement the accuracy results for highly oscillatory coefficients, we examine the numerical conditioning of the reduced operator $\mathcal{A} = B^T AB$ on a fixed grid with $m = 256$. The objective is to assess whether highly oscillatory coefficient or the choice of discrete projection Π_h affect the stability of the reduced system in practice. Two constructions of the discrete spectral basis are compared: direct nodal interpolation of the Laplacian eigenfunctions into V_h (denoted *interp*), and a mass-based projection surrogate (denoted *proj*). In both cases, the resulting basis is mass-orthonormalized so that $B^T MB = I$ to eliminate scaling effects and isolating the intrinsic conditioning of \mathcal{A} .

M	K	$\kappa(\mathcal{A})$ (interp)	$\kappa(\mathcal{A})$ (proj)	L_2 error
2	4	4.0005×10^0	4.0005×10^0	6.2655×10^{-6}
4	16	1.6209×10^1	1.6209×10^1	6.5030×10^{-6}
6	36	3.6540×10^1	3.6540×10^1	1.3553×10^{-5}
8	64	6.6828×10^1	6.6828×10^1	3.3947×10^{-5}
12	144	1.5963×10^2	1.5963×10^2	7.4605×10^{-5}
16	256	2.9043×10^2	2.9043×10^2	8.0390×10^{-5}

TABLE 4. Condition numbers of \mathcal{A} and L_2 errors on a fixed grid $m = 256$.

The results in Table 4 show that $\kappa(\mathcal{A})$ exhibits a moderate, monotone growth as the reduced dimension K increases. This behavior is expected, since enlarging the spectral subspace introduces higher-frequency components into the reduced operator. Importantly, the conditioning remains entirely insensitive to the underlying mesh resolution and is essentially identical for the two discrete projection surrogates once mass-orthonormalization is applied. This confirms the theoretical result that the conditioning of the reduced operator is governed by the bilinear form and basis normalization, rather than by the finite element discretization or the particular realization of Π_h .

7. Conclusions

This work has introduced a spectral low-mode reduced method for the efficient solution of variable-coefficient elliptic boundary value problems. The method is based on projecting a standard finite difference or finite element discretization onto a global coarse space spanned by low Dirichlet Laplacian eigenmodes. Unlike classical spectral discretizations, the differential operator is assembled entirely in physical space, and the spectral basis is used solely as an analytic compression mechanism. As a result, the full heterogeneity of the diffusion coefficient is retained exactly through the projected operator, while the dimensionality of the resulting linear system is reduced by several orders of magnitude.

Theoretical analysis shows that the reduced solution is the energy-optimal Galerkin approximation in the chosen spectral subspace and that the associated error is governed by the decay of Laplacian eigen-coefficients. Under standard elliptic regularity assumptions, the contribution of discarded high modes is shown to decay at a rate proportional to $\sqrt{\log M}/M$, and for uniformly stable reduced bases the projected operator is well conditioned with bounds independent of mesh refinement. A Schur complement interpretation further clarifies the effect of neglecting high-frequency interactions and provides explicit bounds on the truncation error in terms of coefficient regularity.

Numerical experiments confirm the theoretical predictions. For smooth and highly oscillatory diffusion coefficients alike, the reduced solver reproduces the second-order accuracy of the underlying finite difference scheme while maintaining a fixed reduced dimension. In all tested cases, a small number of spectral modes is sufficient to recover full fine-grid accuracy, and increasing the cutoff beyond this point yields diminishing returns, consistent with the analytic error estimates. Runtime comparisons demonstrate that the reduced solver achieves substantial speedups over sparse direct solvers and, in the experiments reported (for the oscillatory coefficient and with the GMG and deflation implementations and parameters used), exhibits favorable performance relative to multigrid and deflation-based Krylov methods.

The results indicate that global Laplacian eigenmodes provide an effective and compact coarse space for elliptic problems with heterogeneous coefficients. By avoiding iterative tuning, problem-dependent coarse space construction, and eigenvector approximation of the full operator, the proposed approach offers a conceptually simple and powerful solver for elliptic boundary-value problems.

References

- [1] I. BABUŠKA AND J. OSBORN, *Eigenvalue problems*, Handbook of Numerical Analysis, II (1991), pp. 641–787.
- [2] M. BENZI, *Preconditioning techniques for large linear systems*, Journal of Computational Physics, 182 (2002), pp. 418–477.
- [3] M. BENZI AND M. TŮMA, *A comparative study of sparse approximate inverse preconditioners*, Applied Numerical Mathematics, 30 (2000), pp. 305–340.
- [4] J. BOYD, *Chebyshev and Fourier Spectral Methods*, Dover, 2001.
- [5] A. BRANDT, *Multi-level adaptive solutions to boundary-value problems*, Mathematics of Computation, 31 (1977), pp. 333–390.
- [6] W. L. BRIGGS, V. E. HENSON, AND S. F. MCCORMICK, *A Multigrid Tutorial*, SIAM, 2000.
- [7] C. CANUTO, M. HUSSAINI, A. QUARTERONI, AND T. ZANG, *Spectral Methods*, Springer, 2006.
- [8] P. G. CIARLET, *The Finite Element Method for Elliptic Problems*, North-Holland, 1978.
- [9] T. A. DAVIS, *Direct Methods for Sparse Linear Systems*, SIAM, 2006.
- [10] H. ELMAN, D. SILVESTER, AND A. WATHEN, *Finite Elements and Fast Iterative Solvers*, Oxford University Press, 2014.
- [11] L. C. EVANS, *Partial Differential Equations*, American Mathematical Society, 2010.
- [12] A. GEORGE, *Nested dissection of sparse matrices*, SIAM Journal on Numerical Analysis, 10 (1973), pp. 345–363.
- [13] J. GILBERT AND J. LIU, *Elimination structures for 2d finite-element matrices*, SIAM Journal on Matrix Analysis and Applications, 14 (1993), pp. 334–352.
- [14] P. GRISVARD, *Elliptic Problems in Nonsmooth Domains*, Pitman, 1985.
- [15] K. KUNISCH AND S. VOLKWEIN, *Galerkin proper orthogonal decomposition methods for a general equation in fluid dynamics*, SIAM Journal on Numerical Analysis, 40 (2002), pp. 492–515.

- [16] R. LIPTON, D. ROSE, AND R. TARJAN, *Generalized nested dissection*, SIAM Journal on Numerical Analysis, 16 (1979), pp. 346–358.
- [17] T. MANTEUFFEL, *An incomplete factorization technique for positive definite linear systems*, Mathematics of Computation, 34 (1980), pp. 473–497.
- [18] W. MCLEAN, *Strongly Elliptic Systems and Boundary Integral Equations*, Cambridge University Press, 2000.
- [19] Y. NOTAY, *An aggregation-based algebraic multigrid method*, Electronic Transactions on Numerical Analysis, 37 (2009), pp. 123–146.
- [20] A. QUARTERONI AND G. ROZZA, *Reduced Basis Methods for Partial Differential Equations*, Springer, 2014.
- [21] A. QUARTERONI AND A. VALLI, *Numerical Approximation of Partial Differential Equations*, Springer, 2008.
- [22] Y. SAAD, *A flexible inner–outer preconditioned gmres algorithm*, SIAM Journal on Scientific Computing, 14 (1993), pp. 461–469.
- [23] Y. SAAD, *Iterative Methods for Sparse Linear Systems*, SIAM, 2003.
- [24] G. STRANG AND G. FIX, *An Analysis of the Finite Element Method*, Prentice-Hall, 1973.
- [25] A. TOSELLI AND O. WIDLUND, *Domain Decomposition Methods*, Springer, 2005.
- [26] L. N. TREFETHEN, *Spectral Methods in MATLAB*, SIAM, 2000.
- [27] C. VUIK, A. SEGAL, AND J. MEIJERINK, *An efficient preconditioner for the incompressible navier–stokes equations*, International Journal for Numerical Methods in Fluids, 31 (1999), pp. 535–550.
- [28] G. WITTUM, *On the robustness of multigrid*, Numerische Mathematik, 61 (1992), pp. 467–488.
- [29] J. XU AND L. ZIKATANOV, *The method of alternating projections and the method of subspace corrections*, SIAM Review, 44 (2002), pp. 247–266.